Magnetic Nanoparticle Clusters

DOI: 10.1002/anie.201408593

Size-Controlled Construction of Magnetic Nanoparticle Clusters Using DNA-Binding Zinc Finger Protein**

*Yiseul Ryu, Zongwen Jin, Joong-jae Lee, Seung-hyun Noh, Tae-Hyun Shin, Seong-Min Jo, Joonsung Choi, HyunWook Park, Jinwoo Cheon, and Hak-Sung Kim**

Abstract: *Nanoparticle clusters (NPCs) have attracted significant interest owing to their unique characteristics arising from their collective individual properties. Nonetheless, the construction of NPCs in a structurally well-defined and size-controllable manner remains a challenge. Here we demonstrate a strategy to construct size-controlled NPCs using the DNA-binding zinc finger (ZnF) protein. Biotinylated ZnF was conjugated to DNA templates with different lengths, followed by incubation with neutravidin-conjugated nanoparticles. The sequence specificity of ZnF and programmable DNA templates enabled a size-controlled construction of NPCs, resulting in a homogeneous size distribution. We demonstrated the utility of magnetic NPCs by showing a three-fold increase in the spin–spin relaxivity in MRI compared with Feridex. Furthermore, folate-conjugated magnetic NPCs exhibited a specific targeting ability for HeLa cells. The present approach can be applicable to other nanoparticles, finding wide applications in many areas such as disease diagnosis, imaging, and delivery of drugs and genes.*

Over the years, clustered assemblies of nanoparticles (NPs), such as magnetic nanoparticles (MNPs), gold nanoparticles (AuNPs), and quantum dots (QDs), have gained considerable attention owing to their unusual and distinct characteristics originating from the collective individual properties of the constituting NPs. Nanoparticle clusters (NPCs) have been shown to exhibit changes in their optical, electrophysical, and mechanical properties.[1] The characteristic interparticle-coupled plasmon absorbance of AuNPs was shown to shift toward a lower energy level compared to separated ones.[2] A larger assembly of MNPs tends to diphase the spin of water protons in the surroundings more efficiently than free NPs, leading to enhanced spin–spin relaxation times.[3]

A hierarchical organization of NPs in a well-defined ensemble is a critical factor that influences the collective property of the clusters. Many approaches have attempted to construct NPCs in a size- and shape-controlled manner.[4] The DNA-directed assembly of NPCs has drawn significant attention,[5] including electrostatic binding of NPs toward a negatively charged phosphate backbone,[6] association of NPs with chemically modified DNA,[7] and base complementation of NPs to single-stranded DNA.[8] However, these approaches require the chemical reduction of metal ions or alteration of the native DNA structure, inevitably limiting the applicable surface functionalities of NPs for further modification. A magnetic nanoworm was constructed using MNPs in a dextran-mediated assembly process.[9] With a high-aspect-ratio geometry, a nanoworm was shown to exhibit more efficient tumor targeting and imaging ability than separated NPs. This approach, however, is likely to be insufficient for constructing diverse shapes of NPCs and controlling their size because such an assembly mainly relies on the interaction with dextran.

Here, we present a strategy to construct NPCs using DNA-binding zinc finger (ZnF) proteins. We reasoned that ZnFs are effective for constructing NPCs in a size-controllable manner through their sequence specificity and easy conjugation to NPs without any additional modification of the template DNA. The sequence specificity and affinity of ZnFs can be easily modulated by varying the numbers of fingers and optimizing the linkers between fingers.[10] A previous study showed site-specific positioning of ZnFs on DNA origami.[11] We used a ZnF, called QNK-QNK-RHR, showing a nanomolar affinity for dsDNA.[10a] To construct NPCs, we first conjugated biotinylated-ZnFs (b-ZnFs) to a DNA template, followed by incubation with neutravidin-conjugated nanoparticles (NA-NPs; Scheme 1a). The size of the NPCs was modulated by changing the length of the DNA template, and the size distribution of the resulting NPCs was examined.

[*] Dr. Y. Ryu,[+] J.-j. Lee, Dr. S.-M. Jo, Prof. H.-S. Kim
Department of Biological Sciences
Korea Advanced Institute of Science and Technology (KAIST)
Daejeon 305-701 (Korea)
E-mail: hskim76@kaist.ac.kr

Dr. Z. Jin[+]
Key Laboratory of Health Informatics
Institute of Biomedical and Health Engineering
Shenzhen Institutes of Advanced Technology (SIAT)
Chinese Academy of Sciences (CAS)
Shenzhen 518055 (China)

S.-h. Noh, T.-H. Shin, Prof. J. Cheon
Department of Chemistry, Yonsei University
Seoul 120-749 (Korea)

Dr. J. Choi, Prof. H. Park
Department of Electrical Engineering
Korea Advanced Institute of Science and Technology (KAIST)
Daejeon 305-701 (Korea)

[+] These authors contributed equally to this work.

[**] We thank Dr. J.-t. Jang and C. Oh for technical support and helpful discussions. This research was supported by the Bio & Medical Technology Development Program (NRF-2013M3A9D6076530), the Mid-career Researcher Program (NRF-2014R1A2A1A01004198) of the National Research Foundation (NRF) funded by the Ministry of Science, ICT & Future Planning, Brain Korea 21 funded by the MOE, and the National Creative Research Initiative (2010-0018286 for J.C.).

Supporting information for this article is available on the WWW under http://dx.doi.org/10.1002/anie.201408593.

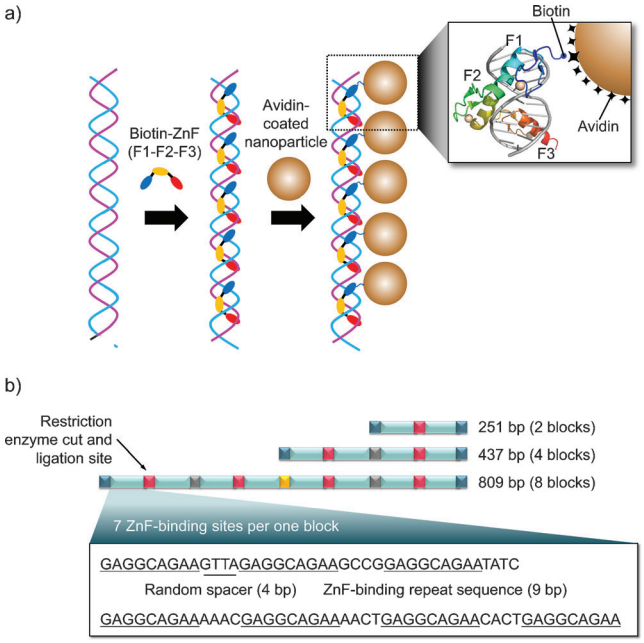

Scheme 1. Construction of NPCs using DNA-binding ZnF protein. a) A schematic representation for the size-controlled construction of NPCs using the DNA template and ZnF protein. Biotinylated ZnF that binds the DNA template consists of three fingers, namely F1, F2, and F3. b) Synthesis of three DNA templates with different lengths through a repeated DNA assembly using restriction enzymes and ligase. The cyan-colored blocks indicate a DNA block as a synthesis unit. The blocks in the other colors indicate the recognition sites of the respective restriction enzyme: red, *NdeI*; gray, *XhoI*; yellow, *SalI*; and blue, *EcoRI*.

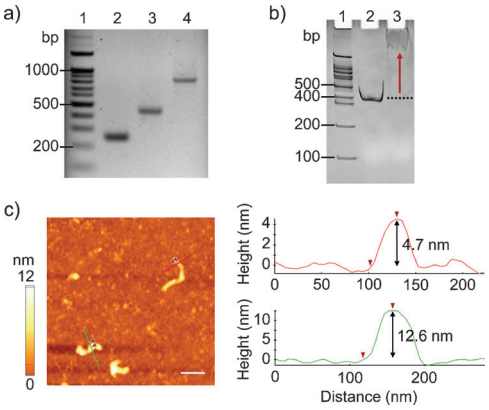

Figure 1. Separation and characterization of the ZnF–DNA complex. a) Agarose gel electrophoresis of three DNA templates. Lane 1: DNA size marker of 100 bp. DNA template of 251 (lane 2), 437 (lane 3), and 809 bp (lane 4). b) Electrophoretic mobility shift assay of b-ZnF for the DNA template of 437 bp. Lane 1: DNA size marker of 100 bp. Lane 2: DNA template of 437 bp. Lane 3: DNA template of 437 bp in complex with ZnF. c) AFM image (left) and selection analysis (right) of the ZnF–DNA complex using a DNA template of 437 bp. Scale bar = 200 nm.

The potential utility of the NPC was investigated in terms of the *T*2 relaxation time and cancer cell targeting ability.

To construct NPCs in a size-controllable manner, we first designed DNA templates with different lengths and multiple ZnF binding sites. DNA templates were designed to contain seven ZnF binding sites flanked by four random base pairs (bp) per one DNA block of 87 bp (Scheme 1 b). Based on the design strategy described in the Supporting Information (SI), three kinds of DNA templates with different lengths, namely 251, 437, and 809 bp, were synthesized to have 14, 28, and 56 ZnF binding sites, respectively (Figures 1 a, Figure S1). The effective lengths of three DNA templates are 180, 366, and 738 bp, respectively, when subtracting 71 bp of adaptor sequence for cloning in each DNA template. Considering the size of MNP used (~ 20 nm including 15 nm of the core MNP, PEG layer, and NA), the maximum number of MNPs that can bind to the DNA templates through a specific interaction is estimated to be 3, 6, and 12, respectively. NPCs were constructed by incubating each DNA template with a molar excess of b-ZnF and subsequently with NA-NPs. In this assembly process, b-ZnF acts as a mediator that links NPs and DNA templates (Figure S2). Unbound ZnF can interfere with the interaction between NA-NPs and DNA templates, and free ZnF was completely removed. The construction of the ZnF–DNA complex could be easily confirmed using a gel shift assay (Figure 1 b). As a complex between ZnF and a DNA template with 437 bp was formed, a band shift was clearly observed. This change in mobility also demonstrates the stability of the formed ZnF–DNA complex, e.g., even after washing steps.

To directly observe the stable association of ZnFs with a DNA template, we investigated the ZnF–DNA complex using atomic force microscopy (AFM). As shown in Figure 1 c and Figure S3, the complexes were found to have various lengths and full width at half maximum (FWHM) values, even though the same DNA template of 437 bp was used. Further analysis revealed that two typical complexes had different dimensions (4.7 nm in height × 29 nm FWHM and 12.6 nm in height × 48 nm FWHM), which were not observed in the presence of a DNA template alone. The difference in morphology is likely to originate from the association of ZnFs with DNA templates. It was reported that naked dsDNA is shown to be 1–2 nm in height in an AFM image.[12] We can therefore rule out the possibility that the morphology difference may be caused by an irregular bending or compaction of dsDNA alone. The rather broad distribution of the complex (lane 3, Figure 1 b) compared to the sharp migration band of naked dsDNA (lane 2) also supports the result of AFM imaging.

To investigate the property of the NPCs, we separated them from free NPs using a density gradient method as described in the SI. The NPCs have a higher specific sedimentation velocity owing to their higher density compared to the free NPs, and the gradient method is effective for separating the NPCs. The loading concentration of the NPCs was shown to be critical to achieve a separation with high purity, and the optimum concentration was determined to be 400 nM with respect to the MNPs. Figure S4 a and b show the optical and TEM images of the separated NPCs and free NPs. The structure of the linear NPCs was distinctively observed in the lower band of the gradient media, and this fraction had few free NPs. The hydrodynamic size of the NPCs was

estimated to be 342 nm based on dynamic light scattering (DLS), whereas that of the free NPs in the upper band was around 50 nm (Figure S4c).

To test whether the NPCs can be constructed in a size-controllable manner, we utilized three kinds of DNA templates with different lengths, namely 251, 437, and 809 bps. Figure 2b shows histograms of the NPCs with respect

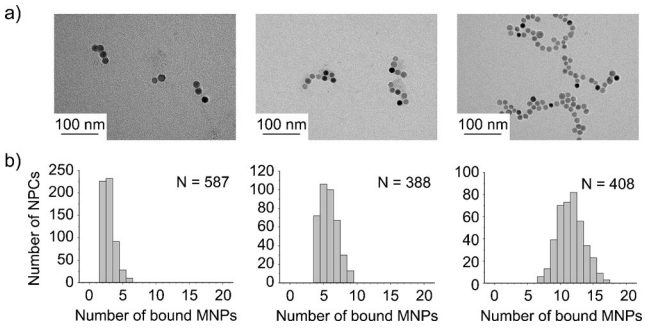

Figure 2. Size-controlled construction of NPCs. a) TEM images, and b) size distribution of constructed NPCs using DNA templates with different lengths, namely 251 bp, 437 bp, and 809 bps. The number of NPCs, N (measured for the respective template) is provided.

to the number of NPs in the respective DNA template. The histograms were obtained by analyzing more than 380 NPCs for each template in the TEM images (Figure 2a, Figure S5). The peak and shape of the distribution histograms were shown to shift as the size of template increased from 251 to 809 bp, demonstrating the construction of NPCs in a size-controllable manner through the change in the length of the DNA template. The average number of MNPs bound to the DNA templates was shown to be 2.9, 5.8, and 11.6, respectively, exhibiting a good agreement with the expected number of MNPs, namely 3, 6, and 12 (Table S1). Standard deviations in the size distribution, however, slightly increased with the increasing length of the DNA template, from 0.9 to 2.0. This seems to be caused by the increased flexibility of a longer DNA, which may interfere with the cluster formation. Based on the results, the present approach can be effectively used for constructing the clusters in a size-controllable manner, showing a generally acceptable range of heterogeneity. High-magnification TEM analysis revealed distinct differences in the cluster structures, depending on the length of the DNA template (Figure 2a).

In an attempt to assess the utility of the NPCs, we evaluated the contrast effect of magnetic NPCs on the *T*2-weighted magnetic resonance imaging (MRI). Figure 3 shows the measurement of the *T*2 relaxation rate ($R2 = 1/T2$) for magnetic NPCs based on the DNA template of 809 bp at different Fe concentrations. As a control, a clinically approved conventional contrast agent, Feridex, was used. As the Fe concentration increased from 0 to 0.25 mM, *R*2 of the magnetic NPCs increased with a three-fold higher slope ($r2 = 315.1\ \mathrm{mM^{-1}s^{-1}}$) than that of Feridex ($r2 = 108.2\ \mathrm{mM^{-1}s^{-1}}$). For a given Fe concentration, the magnetic NPCs resulted in a significantly darker (*T*2-weighted) image than Feridex (inset of Figure 3). Magnetic NPCs showed

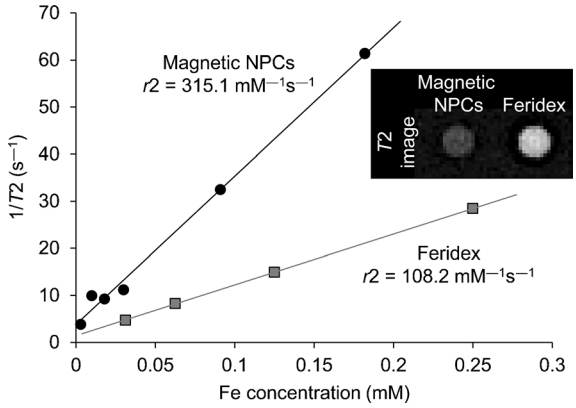

Figure 3. Enhanced MRI contrast effect by magnetic NPCs compared to Feridex. Plots of *R*2 (1/*T*2) versus metal concentration are shown. *T*2 images of the magnetic NPCs and Feridex were obtained using 3.0 T MRI (inset). The concentration of the contrast agents used in the *T*2 images was 0.18 mM (metal).

a slightly higher rate than free MNPs ($r2 = 288\ \mathrm{mM^{-1}s^{-1}}$; Figure S6). A similar result was observed for linearly assembled MNPs using M13 bacteriophage.[13] However, it has been suggested that the potential of magnetic NPCs as an MRI agent should be assessed through in vivo experiments. Clustered nanochains are known to exhibit significantly improved in vivo efficacy compared to isolated NPs owing to their low uptake in the reticuloendothelial system (RES), prolonged blood half-life, and high tumor-targeting ability.[14] The present approach can be extended to other NPs such as QDs and AuNPs, which may bring about unusual physical properties as compared with isolated ones.

We next examined the cellular targeting ability of magnetic NPCs using HeLa cells overexpressing the folate receptor. For this, we conjugated the folate and DNA-intercalating dye (YOYO-1) to the magnetic NPCs as described in the SI. The cells treated with the NPCs exhibited distinct green fluorescence, whereas no fluorescence was observed from the cells treated with the control NPCs (Figure 4). This result clearly demonstrates the receptor-mediated specific uptake of folate-conjugated magnetic NPCs. It is also noteworthy that imaging with DNA-templated NPCs can be easily achieved using a DNA-intercalating dye with a high loading capacity and easy conjugation. Based on the results, the magnetic NPCs are expected to be used as a dual imaging probe with fluorescent and magnetic properties.

In conclusion, we demonstrated a simple and versatile strategy to construct NPCs using DNA-binding ZnF protein. Our approach enables the construction of NPCs in a size-controllable manner through programmable DNA templates and the sequence specificity of ZnF, showing a general applicability to other NPs. The size distribution of the NPCs was well correlated with the length of the DNA template, and the number of MNPs in the NPCs was shown to closely match the expected number. Our results show the potential utility of magnetic NPCs as an enhanced MRI contrast agent and dual probe for magnetic and fluorescence imaging. The present approach can be generally applicable to other NPs such as

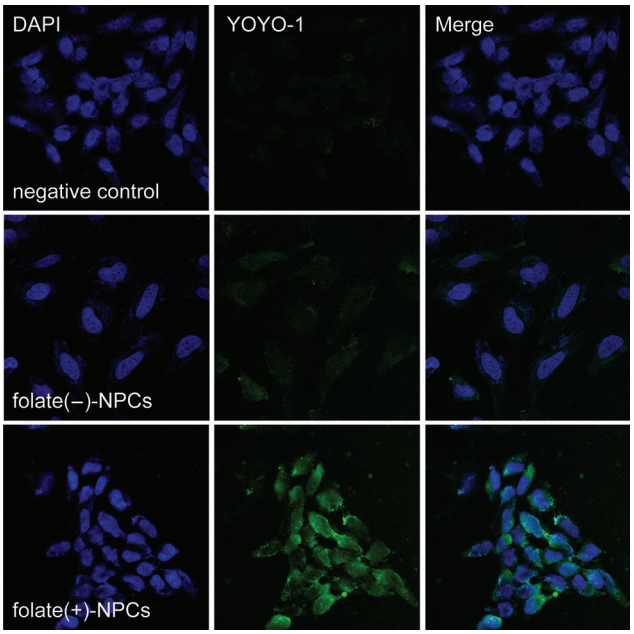

Figure 4. Cellular targeting and uptake of magnetic NPCs. Fluorescence images of HeLa cells treated with media (upper) and magnetic NPCs without (middle) or with (lower) folate. DNA-intercalating dye (YOYO-1)-labelled magnetic NPCs are shown in green. The NPC concentration used was 0.1 nM.

AuNPs and QDs with a slight modification for separation owing to the difference in density. Such NPCs can explore practical applications in many areas such as disease diagnosis and delivery of drugs and genes.[15] Furthermore, elaborate and designable NPC structures can be developed using other types of ZnFs with different sequence specificities for various DNA conformations.

Received: August 27, 2014
Revised: October 13, 2014
Published online: November 25, 2014

Keywords: DNA · nanoparticle clusters · nanostructures · self-assembly · zinc finger

[1] a) E. Katz, I. Willner, *Angew. Chem. Int. Ed.* **2004**, *43*, 6042 – 6108; *Angew. Chem.* **2004**, *116*, 6166 – 6235; b) S. C. Glotzer, *Nat. Mater.* **2003**, *2*, 713 – 714; c) K. Liu, A. Lukach, K. Sugikawa, S. Chung, J. Vickery, H. Therien-Aubin, B. Yang, M. Rubinstein, E. Kumacheva, *Angew. Chem. Int. Ed.* **2014**, *53*, 2648 – 2653; *Angew. Chem.* **2014**, *126*, 2686 – 2691; d) G. A. Devries, M. Brunnbauer, Y. Hu, A. M. Jackson, B. Long, B. T. Neltner, O. Uzun, B. H. Wunsch, F. Stellacci, *Science* **2007**, *315*, 358 – 361.

[2] a) J. Liu, Y. Lu, *J. Am. Chem. Soc.* **2003**, *125*, 6642 – 6643; b) C. A. Mirkin, R. L. Letsinger, R. C. Mucic, J. J. Storhoff, *Nature* **1996**, *382*, 607 – 609; c) N. Pazos-Perez, C. S. Wagner, J. M. Romo-Herrera, L. M. Liz-Marzan, F. J. Garcia de Abajo, A. Wittemann, A. Fery, R. A. Alvarez-Puebla, *Angew. Chem. Int. Ed.* **2012**, *51*, 12688 – 12693; *Angew. Chem.* **2012**, *124*, 12860 – 12865.

[3] a) Z. Jin, Y. K. Hahn, E. Oh, Y.-P. Kim, J.-K. Park, S. H. Moon, J.-T. Jang, J. Cheon, H.-S. Kim, *Small*, **2009**, *5*, 2243 – 2246; b) J. M. Perez, L. Josephson, T. O'Loughlin, D. Hogemann, R. Weissleder, *Nat. Biotechnol.* **2002**, *20*, 816 – 820.

[4] a) L. H. Tan, H. Xing, Y. Lu, *Acc. Chem. Res.* **2014**, *47*, 1881 – 1890; b) L. J. Hill, N. E. Richey, Y. Sung, P. T. Dirlam, J. J. Griebel, E. Lavoie-Higgins, I.-B. Shim, N. Pinna, M.-G. Willinger, W. Vogel, J. J. Benkoski, K. Char, J. Pyun, *ACS Nano* **2014**, *8*, 3272 – 3284; c) C. H. B. Ng, W. Y. Fan, *Langmuir* **2014**, *30*, 7313 – 7318; d) Y. Wang, G. Chen, M. Yang, G. Silber, S. Xing, L. H. Tan, F. Wang, Y. Feng, X. Liu, S. Li, H. Chen, *Nat. Commun.* **2010**, *1*, 87; e) Z. Yin, W. Zhang, Q. Wei Fu, H. Yue, W. Wei, P. Tang, W. Li, W. Li, L. Lin, G. Ma, D. Ma, *Small* **2014**, *10*, 3619 – 3624.

[5] a) L. Y. T. Chou, K. Zagorovsky, W. C. W. Chan, *Nat. Nanotechnol.* **2014**, *9*, 148 – 155; b) A. Kuzyk, R. Schreiber, Z. Fan, G. Pardatscher, E.-M. Roller, A. Hogele, F. C. Simmel, A. O. Govorov, T. Liedl, *Nature* **2012**, *483*, 311 – 314; c) S. M. D. Watson, M. A. Galindo, B. R. Horrocks, A. Houlton, *J. Am. Chem. Soc.* **2014**, *136*, 6649 – 6655.

[6] a) E. Braun, Y. Eichen, U. Sivan, G. Ben-Yoseph, *Nature* **1998**, *391*, 775 – 778; b) O. Harnack, W. E. Ford, A. Yasuda, J. M. Wessels, *Nano Lett.* **2002**, *2*, 919 – 923; c) K. M. Krueger, R. Gilad, G. Ben-Yoseph, U. Sivan, E. Braun, *Science* **2002**, *297*, 72 – 75; d) A. Kumar, M. Pattarkine, M. Bhadbhade, A. B. Mandale, K. N. Ganesh, S. S. Datar, C. V. Dharmadhikari, M. Sastry, *Adv. Mater.* **2001**, *13*, 341 – 344; e) K. Zhang, M. Jiang, D. Chen, *Angew. Chem. Int. Ed.* **2012**, *51*, 8744 – 8747; *Angew. Chem.* **2012**, *124*, 8874 – 8877.

[7] H. Bui, C. Onodera, C. Kidwell, Y. Tan, E. Graugnard, W. Kuang, J. Lee, W. B. Knowlton, B. Yurke, W. L. Hughes, *Nano Lett.* **2010**, *10*, 3367 – 3372.

[8] a) R. Schreiber, J. Do, E.-M. Roller, T. Zhang, V. J. Schuller, P. C. Nickels, J. Feldmann, T. Liedl, *Nat. Nanotechnol.* **2014**, *9*, 74 – 78; b) A. L. Stadler, D. Sun, M. M. Maye, D. van der Lelie, O. Gang, *ACS Nano* **2011**, *5*, 2467 – 2474; c) Y. Zhang, F. Lu, K. G. Yager, D. van der Lelie, O. Gang, *Nat. Nanotechnol.* **2013**, *8*, 865 – 872.

[9] J. H. Park, G. von Maltzahn, L. Zhang, M. P. Schwartz, E. Ruoslahti, S. N. Bhatia, M. J. Sailor, *Adv. Mater.* **2008**, *20*, 1630 – 1635.

[10] a) D. Jantz, J. M. Berg, *Proc. Natl. Acad. Sci. USA* **2004**, *101*, 7589 – 7593; b) J. S. Kim, C. O. Pabo, *Proc. Natl. Acad. Sci. USA* **1998**, *95*, 2812 – 2817.

[11] E. Nakata, F. F. Liew, C. Uwatoko, S. Kiyonaka, Y. Mori, Y. Katsuda, M. Endo, H. Sugiyama, T. Morii, *Angew. Chem. Int. Ed.* **2012**, *51*, 2421 – 2424; *Angew. Chem.* **2012**, *124*, 2471 – 2474.

[12] Z. Liu, Z. Li, H. Zhou, G. Wei, Y. Song, L. Wang, *Microsc. Res. Tech.* **2005**, *66*, 179 – 185.

[13] D. Ghosh, Y. Lee, S, Thomas, A. G. Kohli, D. S. Yun, A. M. Belcher, K. A. Kelly, *Nat. Nanotechnol.* **2012**, *7*, 677 – 682.

[14] P. M. Peiris, L. Bauer, R. Toy, E. Tran, J. Pansky, E. Doolittle, E. Schmidt, E. Hayden, A. Mayer, R. A. Keri, M. A. Griswold, E. Karathanasis, *ACS Nano* **2012**, *6*, 4157 – 4168.

[15] a) L. S. Lin, Z. X. Cong, J. B. Cao, K. M. Ke, Q. L. Peng, J. Gao, H. H. Yang, G. Liu, X. Chen, *ACS Nano* **2014**, *8*, 3876 – 3883; b) M.-K. So, C. Xu, A. M. Loening, S. S. Gambhir, J. Rao, *Nat. Biotechnol.* **2006**, *24*, 339 – 343; c) M. K. Yu, D. Kim, I. H. Lee, J. S. So, Y. Y. Jeong, S. Jon, *Small* **2011**, *7*, 2241 – 2249.

